Available online at www.sciencedirect.com
SCIENCE DIRECT®
Journal of Solid State Chemistry 178 (2005) 2692–2700
JOURNAL OF SOLID STATE CHEMISTRY
www.elsevier.com/locate/jssc

High-pressure synthesis and electrochemical behavior of layered $(1-a)LiNi_{1-y}Al_yO_2 \cdot aLi[Li_{1/3}Ni_{2/3}]O_2$ oxides

E. Shinova[a], E. Zhecheva[a,*], R. Stoyanova[a], G.D. Bromiley[b,c], R. Alcántara[d], J.L. Tirado[d]

[a]*Institute of General and Inorganic Chemistry, Bulgarian Academy of Sciences, 1113 Sofia, Bulgaria*
[b]*Bayerisches Geoinstitut, Universität Bayreuth, D-95440 Bayreuth, Germany*
[c]*Department of Earth Sciences, University of Cambridge, Cambridge CB2 3EQ, UK*
[d]*Laboratorio de Química Inorgánica, Facultad de Ciencias, Universidad de Córdoba, 14071 Córdoba, Spain*

Received 1 April 2005; received in revised form 27 May 2005; accepted 5 June 2005
Available online 19 July 2005

Abstract

Layered $(1-a)LiNi_{1-y}Al_yO_2 \cdot aLi[Li_{1/3}Ni_{2/3}]O_2$ oxides, $0 \leqslant a < 0.4$, have been prepared by solid state reaction between NiO, Al_2O_3 and Li_2O_2 under high pressure. The structural characterization of the layered oxides was performed using powder XRD, IR spectroscopy and EPR spectroscopy at 9.23 and 115 GHz. It has been found that the high-pressure favors Al substitution for Ni in the NiO_2-layers of layered $LiNiO_2$. A random Al/Ni distribution in the layer was found. The incorporation of extra Li in the $Ni_{1-y}Al_yO_2$-layer starts at a precursor composition $Li/(Ni+Al) > 1.2$. While pure NiO_2-layers are able to incorporate under high-pressure up to 1/3Li, the appearance of Al in the NiO_2-layers hinders Li^+ dissolution ($Li < (1-y)/3$). In addition, with increasing Al content there is a strong cationic mixing between the layers. High-frequency EPR of Ni^{3+} indicates that the structural interaction of $LiAl_yNi_{1-y}O_2$ with $Li[Li_{1/3}Ni_{2/3}]O_2$ proceeds via the formation of domains comprising different amount of Ni^{3+} ions. The use of $Li_{1.08}Al_{0.09}Ni_{0.83}O_2$ as a cathode material in a lithium ion cells displays a first irreversible Li extraction at 4.8 V, after which a reversible lithium insertion/extraction between 3.0 and 4.5 V is observed on further cycling.

Keywords: Cathode materials; Lithium nickelates; Structural characterization; EPR spectroscopy

1. Introduction

A new family of oxides based on complex solid solutions between layered lithium nickelates, $LiNiO_2$, and monoclinic dilithium oxides, Li_2MO_3 (M = Mn, Ti, Ru) has been considered as perspective cathode materials for lithium-ion batteries [1]. In these oxides, the electrochemically active components are the nickel ions [2,3]. The role of monoclinic Li_2MO_3 is to stabilize the electrochemical performance of layered $LiNiO_2$ in respect of their cycling stability at elevated temperature and extended potential range [4]. Monoclinic Li_2MnO_3 [5], Li_2TiO_3 [6,7] and Li_2RuO_3 [8] have been chosen due to their structural similarity with layered $LiNiO_2$ [4]. The crystal structure of monoclinic Li_2MO_3 can be represented as a layered structure, which is composed of alternating (Li_2)- and (LiM_2)-layers where MO_6-octahedra share common edges. However, the crystal structure of the $LiNiO_2$-Li_2MO_3 system is not clear yet [9,10]. Dahn et al., based on a careful X-ray analysis, suggested that layered $LiNiO_2$ forms solid solutions with Li_2MO_3 over the whole concentration range [9]. Using NMR spectroscopy and TEM analysis, it has been shown by Thackeray et al. that Li_2MO_3 is structurally integrated into layered $LiNiO_2$ yielding composite structures with domains having short-range order [10]. Monoclinic Li_2NiO_3 has been regarded as a structural analogue of monoclinic Li_2MnO_3 [11]. However, contrary to the other monoclinic Li_2MO_3, Li_2NiO_3 has been prepared under 150 bar in an oxygen-rich atmosphere [11]. Recently, solid solutions between

*Corresponding author. Fax: +359 2 870 50 24.
E-mail address: zhecheva@svr.igic.bas.bg (E. Zhecheva).

0022-4596/$ - see front matter © 2005 Elsevier Inc. All rights reserved.
doi:10.1016/j.jssc.2005.06.006

layered $LiNiO_2$ and monoclinic Li_2NiO_3 over the whole concentration range have been prepared under high-pressure in an oxygen-rich atmosphere [12,13]. The formation of the solid solutions has been discussed on the basis of the X-ray analysis, IR and EPR spectroscopy of Ni^{3+} ions, charge compensation being achieved by Ni^{4+} ions [13]. The complexity of the formation of solid solutions has also been demonstrated at the "$NiO–LiNiO_2$" system [14–16]. At low content of Li ($Li/Ni \leqslant 0.45$), a disordered rock-salt structure is formed, while for $0.45 \leqslant Li/Ni \leqslant 1$ lithium and nickel ions show a tendency to order in (111) cubic planes, culminating at $Li/Ni = 1$ in discrete layers of Li and Ni [14,15]. Recently, the system "$NiO–LiNiO_2$ has been considered as a continuous series of mixed crystals of α-$NaFeO_2$-type structure [16].

Another experimental approach to stabilize layered $LiNiO_2$ electrodes in delithiated state is by substitution for Ni with electrochemically inactive elements (such as Mg, Al, Ti etc.). The layered modification of $LiAlO_2$ can react with $LiNiO_2$ to form solid $LiAl_yNi_{1-y}O_2$ solutions within the concentration range of $0 \leqslant y \leqslant 0.5$ [17–23]. The formation of $LiAl_yNi_{1-y}O_2$ solid solutions is extremely sensitive to the synthesis conditions [17–21]. However, while the formation of the complex $LiNiO_2–Li_2MO_3$ oxides leads to increased capacity of $LiNiO_2$ which is delivered at a potential higher than 4.6 V [5–8], the Al-substituted oxides are characterized with a decreased first discharge capacity at the expense of the improved thermal and cycling stability [22].

In this paper, we provide data on the formation of complex layered $(1-a)LiNi_{1-y}Al_yO_2 \cdot aLi[Li_{1/3}Ni_{2/3}]O_2$ oxides. An Al content Al/(Ni + Al) of 0.05 and 0.10 was imposed, following Ref. [24], according to which a promotion effect on the electrochemical behavior can be expected for substitution levels up to 0.05 per formula unit. XRD powder analysis and IR spectroscopy were used for structural characterization of complex oxide systems. The oxidation state of nickel ions was determined by electron paramagnetic resonance (EPR) of Ni^{3+}. The capability of $(1-a)LiNi_{1-y}Al_yO_2 \cdot aLi[Li_{1/3}Ni_{2/3}]O_2$ to extract and insert lithium reversibly was carried out in lithium test cells.

2. Experimental

The $(1-a)LiNi_{1-y}Al_yO_2 \cdot aLi[Li_{1/3}Ni_{2/3}]O_2$ oxides were prepared by a solid state reaction between NiO, Al_2O_3 and Li_2O_2 (Aldrich) at 3 GPa and 700 °C for 2.5 h. High-pressure synthesis was performed using a 1/2 inch end-loaded piston-cylindrical apparatus at the Bayerisches Geoinstitut. Details of high-pressure synthesis are given elsewhere [12,13]. Under high pressure, varying the Li/(Ni + Al) ratio in the initial mixture from 1.0 to 2.0 resulted in the formation of new compositions. To compensate for lithium volatility at 700 °C, a small excess of Li_2O_2 was used. The lithium content of the samples, the mean oxidation state of nickel and the total nickel content were determined by atomic absorption analysis, iodometric titration and complexometric titration, respectively.

X-ray phase analysis was performed using a Philips X' Pert powder diffractometer with monochromatic $CoK\alpha_1$ radiation, and with a Si internal standard. The scan range was $15° \leqslant 2\theta \leqslant 120°$ with a step increment of 0.02°. A Fullprof computer programme was used for the calculations [25]. The diffractometer point zero, the Lorentzian/Gaussian fraction of the pseudo-Voigt peak function, scale factor, the unit cell parameters (a and c), the oxygen parameter (z), the thermal factor for the 3a, 3b and 6c positions, the line half-width parameters and the preferred orientation were determined. The cationic occupancy factors were refined taking into account that the total occupancies of the 3a, 3b and 6c sites are equal to unity.

The IR spectra were recorded with a Nicolet Avatar-32 spectrometer using KBr pellets.

EPR measurements at 9.23 GHz (X-band) were carried out using a ERS 220/Q spectrometer over the temperature range 85–410 K. The g-factors were established with respect to a Mn^{2+}/ZnS standard. The signal intensity was determined by double integration of the experimental EPR spectrum. The high-frequency EPR spectra were recorded on a single-pass transmission EPR spectrometer built in the High-Magnetic Filed Laboratory, Grenoble, France. The frequencies were changed from 95 to 345 GHz using Gunn diodes and their multipliers. The detection of absorption was performed with a bolometer. The recording temperatures were varied from 5 to 300 K using a variable temperature insert (Oxford Instruments).

Electrochemical experiments were carried out in Swagelok-type cells using a MacPile system in galvanostatic and potentiostatic mode. The positive electrode was formed by active material (85%), carbon black and graphite (10%), and PVDF (5%). The negative electrode was Li. The electrolyte was $LiPF_6$ dissolved in EC:DEC supplied by Merck, which soaked Whatman and Celgard separators. Cells were made in a dry box with Ar atmosphere containing less than 1 ppm of oxygen and water. Scan rates were of 10 mV/0.1 h. In order to normalize the potentiostatic results, the current intensities are expressed as mA per gram of electrode active material.

3. Results and discussion

Al-substituted $LiNiO_2$ oxides isostructural with the well-known layered $LiNiO_2$, $Li_{1-\delta}Ni_{1+\delta}O_2$, were prepared under 3 GPa when the Li-to-Ni ratio in the

precursor mixture varied from 1.05 to 1.20. Fig. 1 gives the X-ray diffraction patterns of Al-substituted oxides. The XRD patterns were refined by hexagonal symmetry, space group *R*-3*m*. The structural model comprises Li in 3*b* sites (000.5), Ni and Al in 3*a* sites (000) and oxygen in 6*c* sites (00*z*). It appears that high-pressure synthesis favors Al substitution for Ni in the NiO_2-layers. As in the case of pure $LiNiO_2$ [26], the refinement procedure is improved when small amounts of Ni occupy the alien Li-site. The amount of Ni in the LiO_2 layer (δ) depends on the initial Li/(Ni + Al) ratio, the best stoichiometry corresponding to Li/(Ni + Al) = 1.1: δ = 0.006 and δ = 0.009 for oxides containing 0.05 and 0.10 Al, respectively (Table 1). Under the same preparation conditions, pure $LiNiO_2$ display higher deviation from stoichiometry: δ = 0.014. The replacement of Ni by Al leads to a decrease in the mean Ni–O bond length, which is consistent with the lower ionic radius of Al (Fig. 2). For both Al contents, there is no difference in the mean Li–O bond length. The trigonal distortion of the lattice (given by the *z*-parameter) increased after Al incorporation (Table 1). The increased trigonal distortion, as well as the reduced amount of Ni in the Li-site, indicates stabilization of the layered crystal structure of $LiNiO_2$ by Al. This result is consistent with that established for Al-substituted $LiNiO_2$ obtained under atmospheric pressure [20]. However, it should be noted that, at atmospheric pressure, the influence of synthesis conditions on non-stoichiometry of $LiAl_xNi_{1-x}O_2$ solid solutions (especially for slightly doped oxides) makes this conclusion ambiguous [21].

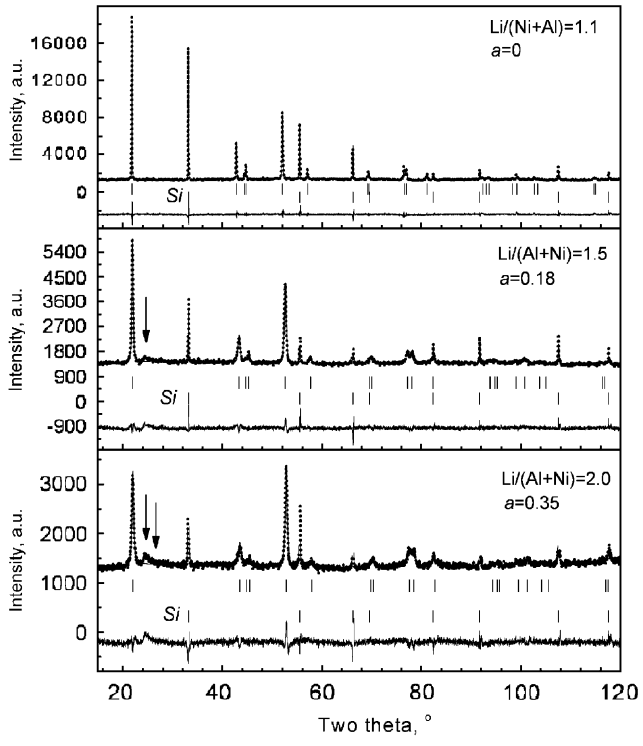

Fig. 1. XRD patterns of $(1-a)LiNi_{1-y}Al_yO_2 \cdot aLi[Li_{1/3}Ni_{2/3}]O_2$ ($y = 0.05$) prepared at 3 GPa from precursors with $1.05 \leqslant Li/(Ni + Al) \leqslant 2.0$. The difference between the observed and calculated profiles is plotted. Bragg reflections for layered hexagonal structure and the Si standard are indicated. The arrows indicate the low-intensity diffuse peaks due to the super-lattice reflections (*C*2/*m*).

By increasing the Li-to-(Ni + Al) ratio above 1.2, the XRD patterns display low-intensity diffuse peaks which are superimposed on the main diffraction lines of the trigonal symmetry (Fig. 1). For these samples, refinement of the XRD diffraction lines was carried out also with a trigonal *R*-3*m* space group, but the structural model included Li on the Ni-site, in addition to a typical $LiNiO_2$ cationic occupancy. The structural parameters are given in Table 1. It appears that incorporation of Li^+ ions in the $Al_yNi_{1-y}O_2$-layers starts at an initial Li/(Ni + Al) > 1.2. The incorporation of Li into the $Al_yNi_{1-y}O_2$-layers is accompanied by an increase in the oxidation state of the Ni ions as determined from chemical analysis. In the same sequence, there is a strong decrease in the unit cell parameters *a* and *c*. In comparison to pure $LiNiO_2$, the amount of Li in the mixed Ni–Al layers is lower than that in the pure nickel layers. Even in the case where a Li-to-(Al + Ni) ratio of 2.0 was used in the precursor mixture, an oxide with a composition $Li_{1.12}Al_{0.05}Ni_{0.83}O_2$ (Li/(Al + Ni) = 1.2) was obtained. In addition, a strong cationic mixing appears when both Al^{3+} and Li^+ reside in the nickel layer. (Fig. 2, Table 1). This result indicates an unfavorable effect of Al on the formation of $LiNiO_2$–Li_2NiO_3 solid solutions with layered structure. The same effect was established for Li_2TiO_3 in the $LiNiO_2 \cdot xLi_2TiO_3$ system [6,7]: the cationic disorder between layers increases with the Ti content, culminating at $x = 0.5$ in the rocksalt structure (*Fm*3*m* space group).

The Li/(Al + Ni) distribution in the compositions can be monitored by infrared spectroscopy (Fig. 3). According to numerous IR study of lithium nickelates, the almost stoichiometric $Li_{1-\delta}Ni_{1+\delta}O_2$ sample ($\delta < 0.02$) exhibits two intense peaks at 500 and 565 cm^{-1} due to NiO_2-vibrations [27–29]. Contrary, the IR spectrum of the monoclinic $Li[Li_{1/3}Ni_{2/3}]O_2$ displays 5 components between 425 and 650 cm^{-1}, which is consistent with the Li/Ni ordering in the mixed $[Li_{1/3}Ni_{2/3}]O_2$ layers as observed from the XRD analysis [13]. Insertion of Al in layered $LiNiO_2$ affects only positions of the two intensive IR modes (Fig. 3). The samples, which contain in addition Li in the Ni-layer, display splitting of the two main IR bands (Fig. 3). In contrast to the IR profile of pure $Li[Li_{1/3}Ni_{2/3}]O_2$, there is a broadening of the IR modes for Al-containing oxides. This broadening can be related to the increased amount of ions that are exchanged between the layers in the $(1-a)LiAl_yNi_{1-y}O_2 \cdot aLi[Li_{1/3}Ni_{2/3}]O_2$ compositions. The effect of the cationic mixing in non-stoichiometric $Li_{1-x}Ni_{1+x}O_2$ on the IR profile is well demonstrated:

Table 1
Structural parameters determined from XRD Rietveld refinement for layered $(1-a)LiNi_{1-y}Al_yO_2 \cdot aLi[Li_{1/3}Ni_{2/3}]O_2$ compositions obtained at high-pressure from precursors with Li-to-(Ni + Al) ratios between 1.05 and 2.0

Initial Li/(Ni + Al)	Initial Al/(Ni + Al)	a/Å (±0.0003)	c/Å (±0.0010)	z, oxygen parameter	δ, ±0.003	x ±0.005	y ±0.005	Ni $1+\delta-x-y$	g	ΔH_{pp}, mT (103 K)	$d\Delta H_{pp}/dT$, mT/K
1.05	0.05	2.8761	14.1954	0.2586	0.038	0	0.046	0.99	2.136	154.3	0.452
1.10	0.05	2.8742	14.1880	0.2592	0.006	0	0.052	0.95	2.126	168.5	0.368
1.5	0.05	2.8387	14.1067	0.2583	0.055	0.114	0.051	0.89	2.085	283.7	–
2.0	0.05	2.8280	14.0733	0.2575	0.075	0.193	0.049	0.83	2.08	278.7	–
1.05	0.10	2.8722	14.2108	0.2586	0.051	0	0.105	0.95	2.095	163.1	0.410
1.10	0.10	2.8720	14.2007	0.2596	0.009	0	0.098	0.91	2.095	175.1	0.360
1.5	0.10	2.8498	14.1459	0.2582	0.041	0.130	0.095	0.81	2.090	231.9	0.183
1.5	0.10	2.8458	14.1233	0.2579	0.060	0.140	0.090	0.83	2.092	255.5	–
2.0	0.10	2.8295	14.0638	0.2575	0.077	0.158	0.098	0.82	2.070	250.9	–

The values of δ, x and y were obtained for a formula unit $(Li_{1-\delta}Ni_\delta)_{3b}[Li_xNi_{1-x-y}Al_y]_{3a}O_2$. Total Ni-content, g-Factor, EPR line width determined at 103 K in the X-band (ΔH_{pp}, mT) and the slope of the temperature dependence of the EPR line width, ($d\Delta H_{pp}/dT$, mT/K) are given in the last four columns.

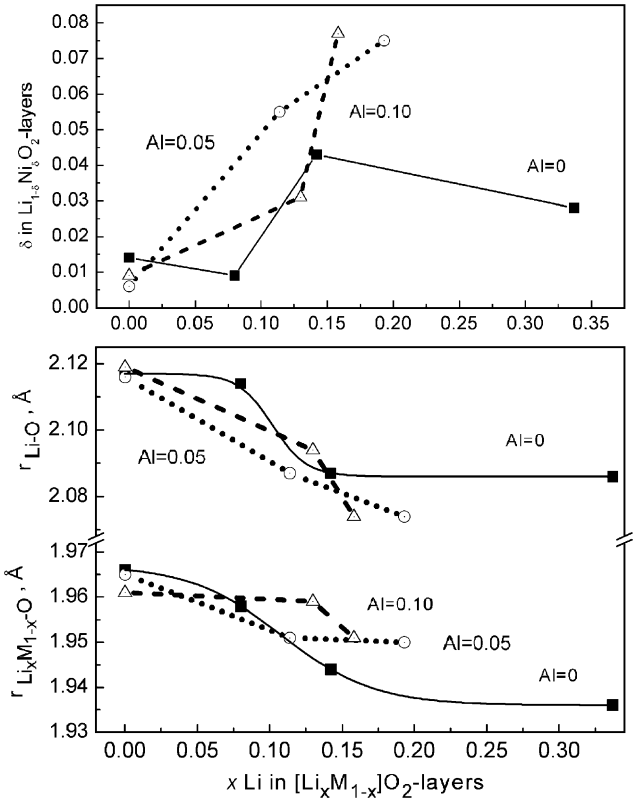

Fig. 2. Mean $Li_xNi_{1-x-y}Al_y$–O and Li–O bond lengths, as well as the amount of cationic mixing between the layers, δ, versus amount of Li in the mixed $[Li_xNi_{1-x-y}Al_y]O_2$-layers.

by increasing the amount of Ni in the Li site the two characteristic IR modes merge into one featureless band [29]. However, the increased number of IR modes in $(1-a)LiAl_yNi_{1-y}O_2 \cdot aLi[Li_{1/3}Ni_{2/3}]O_2$ spectra provides evidence for additional short-range ordering of lithium and nickel at these compositions.

The oxidation state of nickel ions and cationic distribution in the oxides were studied by EPR spectroscopy at 9.3 GHz (X-band). Fig. 4 compares the EPR spectra from $(1-a)LiNi_{1-y}Al_yO_2 \cdot aLi[Li_{1/3}Ni_{2/3}]O_2$ oxides. Nearly stoichiometric $LiNiO_2$ has an EPR spectrum consisting of a single line with Lorentzian shape and $g = 2.137$ due to exchange-coupled Ni^{3+} ions. In the EPR spectrum of Al-substituted non-stoichiometric lithium nickelates, $Li_{1-\delta}Ni_\delta[Ni]O_2$, there is a broad Lorentzian line. The substitution of aluminium for nickel, $Li_{1-\delta}Ni_\delta[Ni_{1-y}Al_y]O_2$, affects essentially the g factor and the line width (Table 1). The g-factor decreases after replacement of Ni by Al, indicating an increased covalency of the Ni–O bond. In the same sequence, diamagnetic Al ions cause line broadening due to the suppression of the exchange interactions between Ni^{3+} ions. The same effect has been found for Al-substituted lithium nickelates obtained under atmospheric pressure [20]. Thus, the observed effect of Al on the g-factor and on the line width of Ni^{3+} ions indicates the formation of solid solution between $LiAlO_2$–$LiNiO_2$ under high pressure. This is consistent with the XRD data (Fig. 1 and Table 1).

The temperature variation of the EPR line width is also affected by the Al substitution (Fig. 5). For pure $Li_{1-\delta}Ni_{1+\delta}O_2$ oxides, the signal shows a linear increase of the line width with the registration temperature within the range 100–400 K. The $d\Delta H_{pp}/dT$ slope has been shown to depend on the strength of the 180°- and 90°-$Ni^{3+/2+}$–O–$Ni^{3+/2+}$ exchange interaction, the coordination number of the exchange-coupled particles and on the distance between them [30,31]. The slope of the linear dependence, $d\Delta H_{pp}/dT$, decreases with the reduction of the amount of Ni^{2+} in the lithium layers: from 0.492 to 0.421 mT/K for $Li_{1-\delta}Ni_{1+\delta}O_2$ with $\delta = 0.055$ and $\delta = 0.014$, respectively. Further decrease in $d\Delta H_{pp}/dT$ is observed when Al substitutes for Ni, $Li_{1-\delta}Ni_\delta[Al_yNi_{1-y}]O_2$ (Table 1). This result also demon-

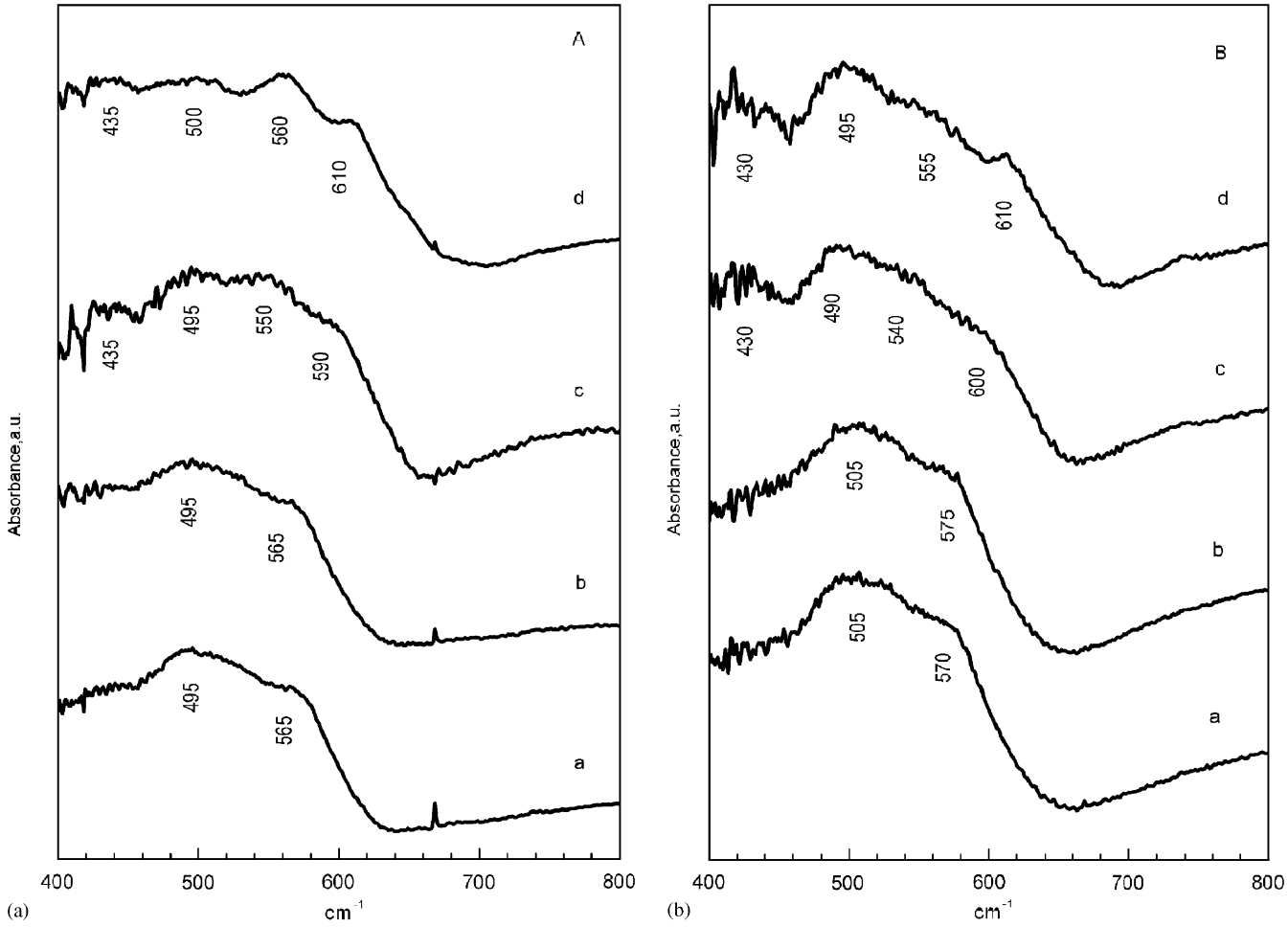

Fig. 3. IR spectra of $(1-a)LiNi_{1-y}Al_yO_2 \cdot aLi[Li_{1/3}Ni_{2/3}]O_2$, $y = 0.05$ (A) and 0.10 (B), prepared at 3 GPa from precursors with Li/(Ni + Al) ratios: (a) 1.05; (b) 1.10; (c) 1.5, and (d) 2.0. The corresponding a-value are as follows: A—(a) $a = 0$; (b) $a = 0$; (c) $a = 0.18$ and (d) $a = 0.35$; B—(a) $a = 0$; (b) $a = 0$; (c) $a = 0.27$ and (d) $a = 0.24$.

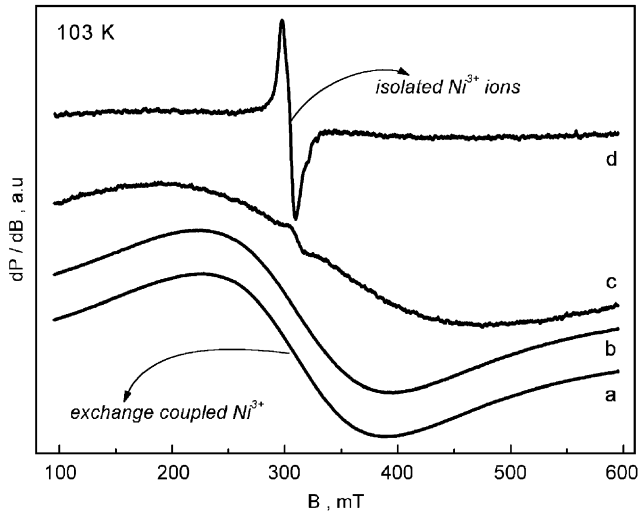

Fig. 4. EPR spectra in X-band of $(1-a)LiNi_{1-y}Al_yO_2 \cdot aLi[Li_{1/3}Ni_{2/3}]O_2$ ($y = 0.05$) prepared at 3 GPa from precursors with a Li/(Ni + Al) ratio of (a) 1.05 ($a = 0$); (b) 1.10 ($a = 0$); (c) 1.5 ($a = 0.18$), and (d) 2.0 ($a = 0.35$).

strates the formation of solid solutions between $LiAlO_2$ and $LiNiO_2$. Moreover, these solid solutions are characterized by minimum amount of Ni ions in LiO_2-layers. A reduction of the Ni occupancy in the Li-site has been also established for Ga-substituted $LiNiO_2$ obtained under high-pressure [32].

When Li is incorporated in the mixed $Al_yNi_{1-y}O_2$-layers, there is a further increase in the line width (Fig. 5). In addition, a low-intensity narrow line superimposed on the main broad signal is resolved for samples with lithium content in the $Al_yNi_{1-y}O_2$-layers higher than 0.1 (Fig. 4). This means that magnetically isolated Ni^{3+} ions exist in a diamagnetic environment in these compositions. It is worth recalling that in $(1-a)LiNi_{1-y}Al_yO_2 \cdot aLi[Li_{1/3}Ni_{2/3}]O_2$ oxides only Ni^{3+} is paramagnetic, while Li^+, Ni^{4+} and Al^{3+} are diamagnetic.

Additional differentiation between the samples containing lithium in the nickel layers can be achieved by EPR spectroscopy at high frequencies. The higher resolution of the high-frequency EPR as compared to the conventional X-band EPR has been demonstrated

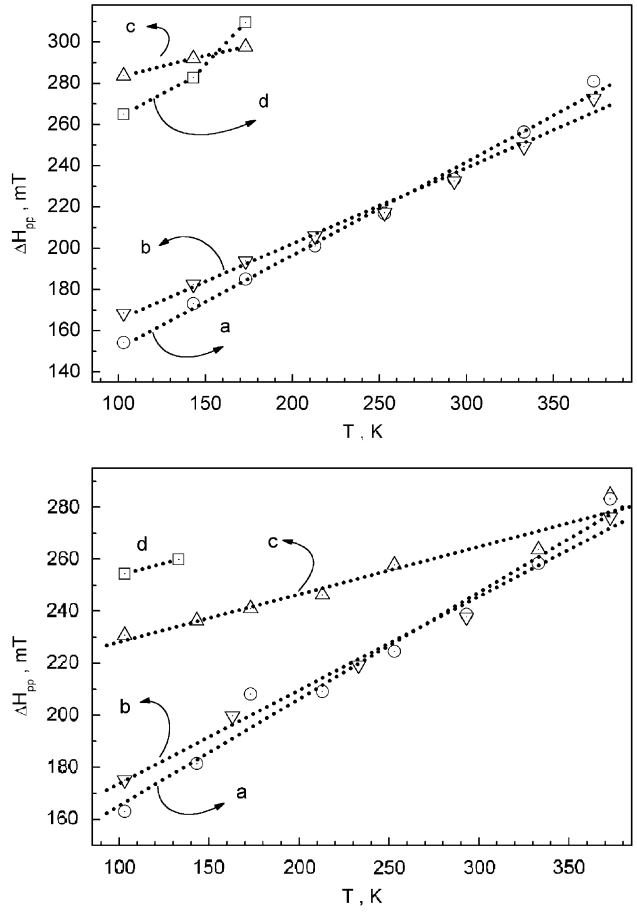

Fig. 5. Temperature variation of the EPR line width of $(1-a)LiNi_{1-y}Al_yO_2 \cdot aLi[Li_{1/3}Ni_{2/3}]O_2$, $y = 0.05$ and 0.10 (top and bottom), prepared at 3 GPa from precursors with Li/(Ni + Al) ratios between 1.05 and 2.0. (Sample notation as in Fig. 4).

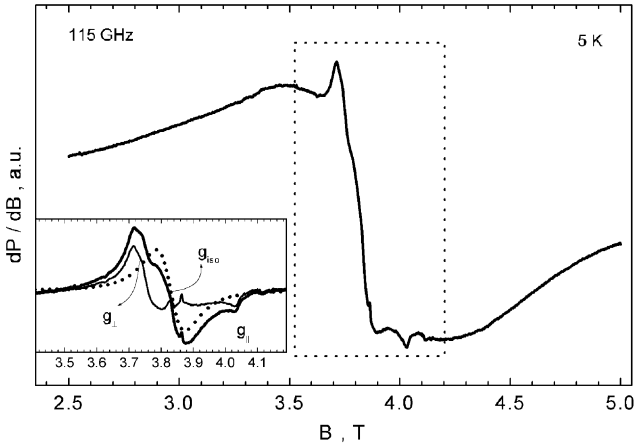

Fig. 6. EPR spectra at 115 GHz for $Li_{1.12}Al_{0.05}Ni_{0.83}O_2$.

for $Li_{1-\delta}Ni_{1+\delta}O_2$ with $0.02 \leqslant \delta \leqslant 0.12$ [33], as well as for Ni^{3+} spin probes in layered $LiAl_xCo_{1-x}O_2$ matrix [34]. The high-frequency spectrum of $Li_{1.12}Al_{0.05}Ni_{0.83}O_2$ displays at 5 K three overlapping EPR signals (Fig. 6). A main signal with an asymmetric shape and line width of about 1.4 T is clearly resolved. This signal has parameters close to those of Ni^{3+} in $Li[Li_{0.14}Ni_{0.86}]O_2$ [13]. The similar EPR parameters indicate that the signal comes from Ni^{3+} ions in mixed Ni^{3+}/Ni^{4+} environment. The other two signals have a low-intensity as compared to the main broad signal. The appearance of these latter signals can be associated with Ni^{3+} ions having different local environment in respect to Ni^{3+} and Al^{3+}/Ni^{4+} ions. One of them is a single Lorentzian line with $g = 2.144$ and a line width of 89 mT. Taking into account the EPR results on $LiAl_xNi_{1-x}O_2$ solid solutions obtained at atmospheric pressure, this low intensity Lorentzian line can be assigned to Ni^{3+} ions having mainly diamagnetic Al^{3+} neighbors and small amount of paramagnetic Ni^{3+} ions [20]. The other low-intensity signal has a line with an axially symmetry: $g_{\parallel} = 2.038$ and $g_{\perp} = 2.196$. The axially symmetric line indicates that this signal comes from Ni^{3+} located in diamagnetic ions environment. For the sake of comparison, low-spin Ni^{3+} ions in diamagnetic $LiAlO_2$ and $LiCoO_2$ are characterized with a tetragonal symmetric g-tensor [34]: $g_{\perp} = 2.1610$, $g_{\parallel} = 2.0379$ and $g_{\perp} = 2.1759$, $g_{\parallel} = 2.0739$ for Ni^{3+} in a Al_6- and Co_6-shell, respectively. The progressive replacement of Co by Al has been shown to cause the smooth decrease in the value of $g_{\perp}$ from 2.2 to 2.16 [34]. In the case of $(1-a)LiNi_{1-y}Al_yO_2 \cdot aLi[Li_{1/3}Ni_{2/3}]O_2$, the observed values of the g-tensor indicate that the magnetically isolated Ni^{3+} ions are rather surrounded by diamagnetic Ni^{4+} than by Al^{3+}.

The detection of tree types of Ni^{3+} ions in $(1-a)LiAl_yNi_{1-y}O_2 \cdot aLi[Li_{1/3}Ni_{2/3}]O_2$ underlines the ability of HF–EPR to assess the local environment of paramagnetic ions, which is not possible to evaluate by conventional X-band EPR. In addition, the detection of tree types of Ni^{3+} ions demonstrates that structure interaction of $LiAl_yNi_{1-y}O_2$ with $Li[Li_{1/3}Ni_{2/3}]O_2$ proceeds via the formation of domains characterized with a different amount of Ni^{3+} ions. Unfortunately, a quantitative analysis of the composition of these domains, as well as their dimensions, is not possible to evaluate by EPR. Formation of a local domain structure has also been established by NMR and TEM analysis for the complex "$LiNi/MnO_2$–Li_2TiO_3" system [10].

The electrochemical behavior of $(1-a)LiNi_{1-y}Al_yO_2 \cdot aLi[Li_{1/3}Ni_{2/3}]O_2$ solid solutions was essayed for the sample with $Li_{1.08}Al_{0.09}Ni_{0.83}O_2$ stoichiometry. This solid was used as active cathode material in lithium test cells and the potentiostatic results are shown in Fig. 7. After a first irreversible Li extraction at 4.8 V, Figs. 7A and B show reversible lithium insertion/extraction processes between 3.0 and 4.5 V, which prevail on further cycling. It is well established that nearly stoichiometric $LiNiO_2$ displays multiple phase

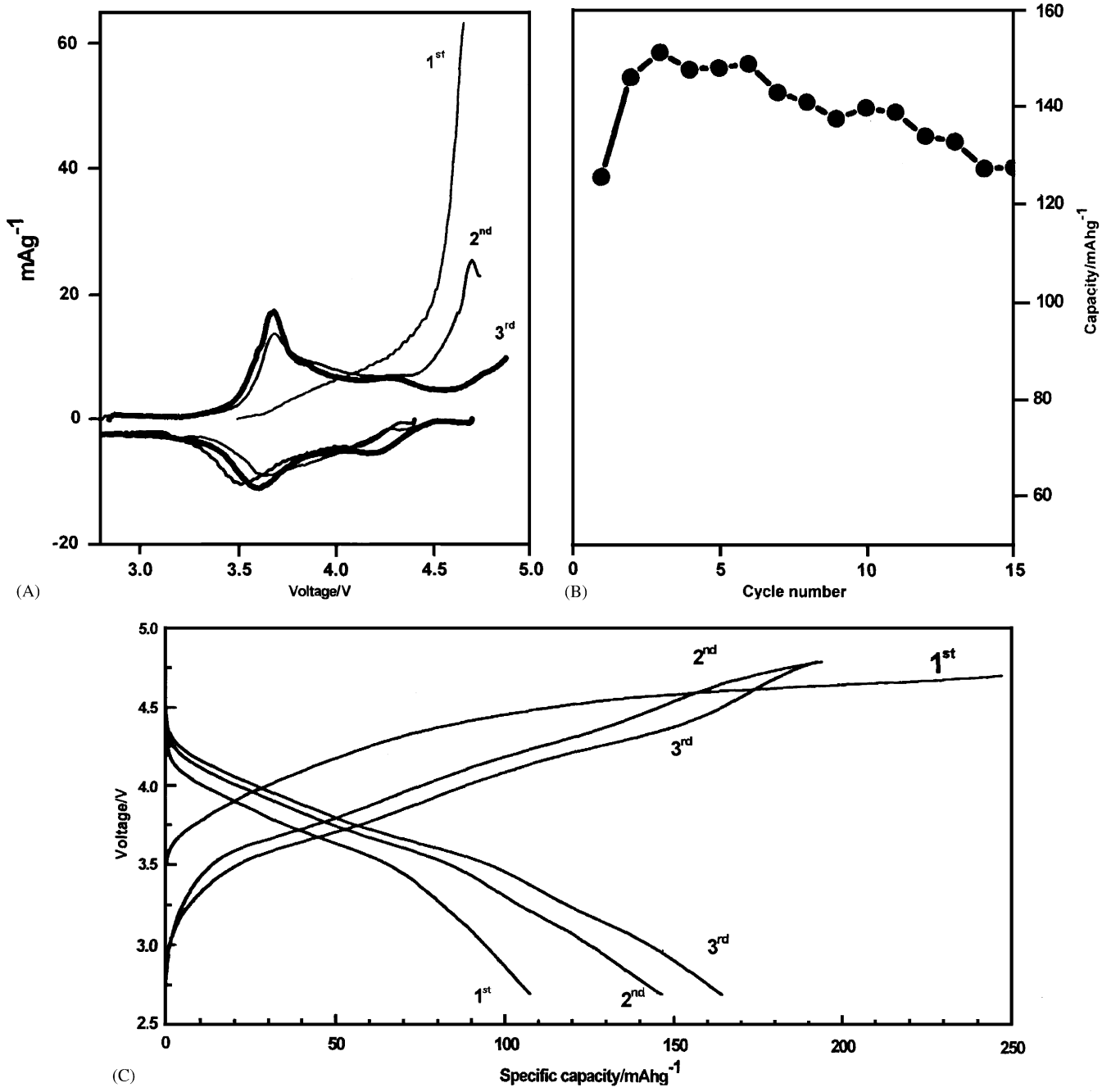

Fig. 7. (A) Normalized intensity (I, in mA g^{-1}) vs. voltage, (B) voltage vs. specific capacity, and (C) capacity vs. cycle number curves from PITT experiments in lithium batteries used $Li_{1.08}Al_{0.09}Ni_{0.83}O_2$.

transitions in the 4-V region [35–38]. The electrochemical behavior of $LiAl_yNi_{1-y}O_2$ samples changes from $y = 0.01$ (similar to $LiNiO_2$) to $y = 0.05$, in which the peaks corresponding to first-order phase transitions become very broad [18]. For $y = 0.1$, lithium-ion diffusion proceeds in a single phase [39]. Finally, for $y = 0.25$, a single-phase mechanism has also been reported [17,40]. Nearly-stoichiometric $LiNiO_2$ obtained at 3 GPa shows an intensity vs. voltage curve with four peaks below 4.5 V [12]. Besides a small difference between the first charge and subsequent cycles, these peaks were maintained upon prolonged cycling. The position of these peaks is close to that observed for nearly-stoichiometric $LiNiO_2$ obtained at atmospheric pressure and can be ascribed to the usual phase transitions [35–38]. However, a sample obtained at 3 GPa with Li excess (initial Li/Ni ratio = 1.5) and refined $Li_{0.96}Ni_{0.04}[Li_{0.19}Ni_{0.81}]O_2$ cation distribution showed a different behavior, with the

presence of an irreversible 4.8 V signal in the voltammogram [12]. The origin of the irreversible high-voltage peak has been ascribed to a simultaneous extraction of lithium and oxygen leading to a solid with a stoichiometry closer to Li_yNiO_2. The absence of multiple phase features in the voltammogram of $Li_{0.94}Ni_{0.06}[Al_{0.09}Li_{0.14}Ni_{0.77}]O_2$ is common to the Al-free $Li_{0.96}Ni_{0.04}[Li_{0.19}Ni_{0.81}]O_2$ material described in the literature [12]. The major difference is an increase in the voltage, at which the peaks develop. In atmospheric pressure samples, the increase in operating cell voltage is observed with Al content in agreement with ab initio calculations [40].

4. Conclusions

In conclusion, high-pressure synthesis in an oxygen rich atmosphere favors the solid state interaction between layered $LiAl_yNi_{1-y}O_2$ and monoclinic Li_2NiO_3, layered $(1-a)LiNi_{1-y}Al_yO_2 \cdot aLi[Li_{1/3}Ni_{2/3}]O_2$ compositions ($0 \leqslant a < 0.4$) being obtained. While pure NiO_2-layers are able to incorporate Li^+ under high-pressure, the ability of Al substituted NiO_2-layers to dissolve Li^+ is limited. In addition, there is a strong cationic mixing with increasing Al content. High-frequency EPR of Ni^{3+} indicates that structure interaction of $LiAl_yNi_{1-y}O_2$ with $Li[Li_{1/3}Ni_{2/3}]O_2$ proceeds via the formation of domains characterized with different amount of Ni^{3+} ions. These composite oxides display different electrochemical properties as compared to Al-substituted $LiNiO_2$. After the first irreversible Li extraction from $Li_{0.94}Ni_{0.06}[Al_{0.09}Li_{0.14}Ni_{0.77}]O_2$ at 4.8 V, a reversible lithium insertion/extraction is achieved on further cycling between 3.0 and 4.5 V.

Acknowledgments

E.Zh., R.S. and E.Sh. acknowledge the National Science Fund of Bulgaria (Contract no. Ch1304/2003) for financial support. E.Sh. is grateful to the EC for a grant of a Marie Curie Host Fellowship Programme (Contract No. HPMT-CT-2001-00231 to D.C. Rubie) in order to perform high-pressure synthesis experiments at the Bayrisches Geoinstitute. The high-frequency EPR measurements carried out at High Magnetic Field Laboratory in Grenoble, France, were supported by European Community "Access to Research Infrastructure action of the Improving Human Potential Programme". The authors are very grateful to Dr. T. Boffa-Ballaran, from Bayerisches Geoinstitut-Universität Bayreuth, and Dr. A.-L. Barra, from High Magnetic Field Laboratory in Grenoble, for their help. JLT and RA thank CICYT for financial support (MAT2002-00434) and program Ramón y Cajal.

References

[1] M.S. Whittingham, Chem. Rev. 104 (2004) 4271.
[2] M.E. Spahr, P. Novak, B. Schneyder, O. Haas, R. Nesper, J. Electrochem. Soc. 145 (1998) 1113.
[3] Z. Lu, J.R. Dahn, J. Electrochem. Soc. 149 (2002) A815.
[4] C.S. Johnson, J.-S. Kim, A.J. Kropf, A.J. Kahaian, J.T. Vaughey, M.M. Thackeray, Electrochem. Commun. 4 (2002) 492.
[5] Z. Lu, L.Y. Bealieu, R.A. Donaberger, C.L. Thomas, J.R. Dahn, J. Electrochem. Soc. 149 (2002) A778.
[6] L. Zhang, T. Muta, H. Noguchi, X. Wang, M. Zhou, M. Yoshio, J. Power Sources 117 (2003) 137.
[7] L. Zhang, X. Wang, H. Noguchi, M. Yoshio, K. Takada, T. Sasaki, Electrochim. Acta 49 (2004) 3305.
[8] G.J. Moore, C.S. Johnson, M.M. Thackeray, J. Power Sources 119 (2003) 216.
[9] Z. Lu, Z. Chen, J.R. Dahn, Chem. Mater. 15 (2003) 3214.
[10] J.-S. Kim, C.S. Johnson, J.T. Vaughey, M.M. Thackeray, S.A. Hackney, W. Yoon, C.P. Grey, Chem. Mater. 16 (2004) 1996.
[11] H.-N. Migeon, A. Courtois, M. Zanne, C. Gleitzer, Rev. Chim. Miner. 13 (1976) 1.
[12] R. Stoyanova, E. Zhecheva, R. Alcántara, J.L. Tirado, G. Bromiley, F. Bromiley, T. Boffa Ballaran, Solid State Ionics 161 (2003) 197.
[13] E. Shinova, E. Zhecheva, R. Stoyanova, G.D. Bromiley, J. Solid State Chem. 178 (2005) 1661.
[14] J.B. Goodenough, D.C. Wickham, W.J. Croft, J. Phys. Chem. Solids 5 (1958) 107.
[15] W. Li, J.N. Reimers, J.R. Dahn, Phys. Rev. B 46 (1992) 3236.
[16] H. Wulf, M. Mohan Rao, F. Scholz, Chem. Mater. 15 (2003) 988.
[17] T. Ohzuku, A. Ueda, M. Kouguchi, J. Electrochem. Soc. 142 (1995) 4033.
[18] O. Zhong, U. von Sacken, J. Power Sources 54 (1995) 221.
[19] T. Ohzuku, T. Yanagawa, M. Kouguchi, A. Ueda, J. Power Sources 68 (1997) 131.
[20] R. Stoyanova, E. Zhecheva, E. Kuzmanova, R. Alcántara, P. Lavela, J.L. Tirado, Solid State Ionics 128 (2000) 1.
[21] M. Guilmard, A. Rougier, M. Grüne, L. Croguennec, C. Delmas, J. Power Sources 115 (2003) 305.
[22] J. Kim, J. Liu, C. Chen, K. Amine, J. Electrochem. Soc. 150 (2003) A1491.
[23] P. Kalyani, N. Kalaiselvi, N.G. Renganathan, M. Raghavan, Mater. Res. Bull. 39 (2004) 41.
[24] G. Pistoia, A. Antolini, R. Rosati, C. Bellitto, G.M. Ingo, Chem. Mater. 9 (1997) 1443.
[25] J. Rodríguez-Carvajal, in: Satellite Meeting on Powder Diffraction of the XV Congress of the IUCr, 1990, p. 127.
[26] A. Rougier, P. Gravereau, C. Delmas, J. Electrochem. Soc. 143 (1996) 1168.
[27] W.W. Huang, R. Frech, Solid State Ionics 86–88 (1996) 395.
[28] C. Julien, Solid State Ionics 136–137 (2000) 887.
[29] E. Zhecheva, R. Stoyanova, Solid State Ionics 66 (1993) 143.
[30] R. Stoyanova, E. Zhecheva, C. Friebel, J. Phys. Chem. Solids 54 (1993) 9.
[31] R. Stoyanova, E. Zhecheva, R. Alcántara, P. Lavela, J.L. Tirado, Solid State Commun. 102 (1997) 457.
[32] R. Stoyanova, E. Zhecheva, R. Alcántara, J.L. Tirado, G. Bromiley, F. Bromiley, T. Boffa Ballaran, J. Mater. Chem. 14 (2004) 3663.
[33] A.-L. Barra, G. Chouteau, A. Stepanov, A. Rougier, C. Delmas, Eur. Phys. J. B 7 (1999) 551.
[34] R. Stoyanova, E. Zhecheva, R. Alcántara, J.L. Tirado, J. Phys. Chem. B 108 (2004) 4053.
[35] T. Ohzuku, A. Ueda, M. Nagayama, J. Electrochem. Soc. 140 (1993) 1862.

[36] W. Lee, J.N. Reimers, J.R. Dahn, Solid State Ionics 67 (1993) 123.
[37] H. Arai, S. Okada, H. Ohtsuka, M. Ichimura, J. Yamaki, Solid State Ionics 80 (1995) 261.
[38] R. Alcántara, P. Lavela, J.L. Tirado, R. Stoyanova, E. Kuzmanova, E. Zhecheva, Chem. Mater. 9 (1997) 2145.
[39] S.H. Park, K.S. Park, Y.K. Sun, K.S. Nahm, Y.S. Lee, M. Yoshio, Electrochim. Acta 46 (2001) 1215.
[40] Y.I. Jang, B. Huang, H. Wang, G.R. Maskaly, G. Ceder, D.R. Sadoway, Y.M. Chiang, H. Liu, H. Tamura, J. Power Sources 81–82 (1999) 589.